Available online at www.sciencedirect.com
ScienceDirect
Geochimica et Cosmochimica Acta 72 (2008) 2636–2648
Geochimica et Cosmochimica Acta
www.elsevier.com/locate/gca

A paired sulfate–pyrite $\delta^{34}S$ approach to understanding the evolution of the Ediacaran–Cambrian sulfur cycle

D.A. Fike [a,b,*], J.P. Grotzinger [b]

[a] Department of Earth, Atmospheric, & Planetary Sciences, Massachusetts Institute of Technology, Cambridge, MA 02139, USA
[b] Division of Geological and Planetary Sciences, California Institute of Technology, Pasadena, CA 91125, USA

Received 16 May 2007; accepted in revised form 18 March 2008; available online 10 April 2008

Abstract

An anomalous enrichment in marine sulfate $\delta^{34}S_{SO_4}$ is preserved in globally-distributed latest Ediacaran–early Cambrian strata. The proximity of this anomaly to the Ediacaran–Cambrian boundary and the associated evolutionary radiation has invited speculation that the two are causally related. Here we present a high-resolution record of paired sulfate ($\delta^{34}S_{SO_4}$) and pyrite ($\delta^{34}S_{pyr}$) from sediments spanning ca. 547–540 million years ago (Ma) from the Ara Group of the Huqf Supergroup, Sultanate of Oman. We observe an increase in $\delta^{34}S_{SO_4}$ from ~20‰ to ~42‰, beginning at ca. 550 Ma and continuing at least through ca. 540 Ma. There is a concomitant increase in $\delta^{34}S_{pyr}$ over this interval from ~−15‰ to 10‰. This globally correlative enrichment, here termed the Ara anomaly, constitutes a major perturbation to the sulfur cycle. The absolute values of $\delta^{34}S_{pyr}$ reported here and in equivalent sections around the world, require the isotopic composition of material entering the ocean ($\delta^{34}S_{in}$) to be significantly more enriched than modern (~3‰) values, likely in excess of 12‰ during the late Ediacaran–early Cambrian. Against this background of elevated $\delta^{34}S_{in}$, the Ara anomaly is explained not by increased fractionation between sulfate and pyrite ($\Delta\delta^{34}S$), but by an increase in pyrite burial (f_{pyr}), most likely driven by enhanced primary production and sequestration of organic carbon, consistent with earlier reports of elevated organic carbon burial and widespread phosphorite deposition.

1. INTRODUCTION

The Ediacaran–Cambrian (E-C) boundary at ca. 541 Million years ago (Ma) (Bowring et al., 2007) marks a period of significant, although still poorly understood, global biogeochemical change, including evidence for ocean anoxia (Kimura and Watanabe, 2001; Schröder and Grotzinger, 2007), the extinction of Ediacaran *Namacalathus* and *Cloudina* fossil assemblages, and a 7‰ negative excursion in the carbon isotopic composition of carbonate minerals ($\delta^{13}C_{carb}$) of ~1 Myr duration (Amthor et al., 2003). We seek additional understanding of this time by examining biogeochemical sulfur cycling. The sulfur cycle, mediated by a variety of microbial processes with distinctive metabolic fractionations (e.g., Habicht et al., 1998), plays a key role in regulating Earth's surface redox balance and serves as a record of ecological variation. As such, understanding sulfur cycling in the latest Ediacaran–early Cambrian may shed light on the biogeochemical changes associated with the E-C boundary. There is ample reason to believe that examining the sulfur cycle may be a productive line of inquiry: an extreme enrichment in marine sulfate $\delta^{34}S_{SO_4}$ has long been recognized in terminal Ediacaran–earliest Cambrian strata (e.g., Thode and Monster, 1965; Holser, 1977; Claypool et al., 1980).

The interval straddling the E-C boundary records an anomalous enrichment in $\delta^{34}S_{SO_4}$ of marine sulfate preserved worldwide in evaporites, phosphorites, and carbonate-associated sulfate (Fig. 1). This enrichment is here termed the Ara anomaly because the onset and peak are extremely well represented in the coeval Ara Group, Sultanate of Oman. Enriched $\delta^{34}S_{SO_4}$ values during the Ara anomaly

* Corresponding author. Fax: +1 626 568 0935.
E-mail address: dfike@gps.caltech.edu (D.A. Fike).

0016-7037/$ - see front matter © 2008 Elsevier Ltd. All rights reserved.
doi:10.1016/j.gca.2008.03.021

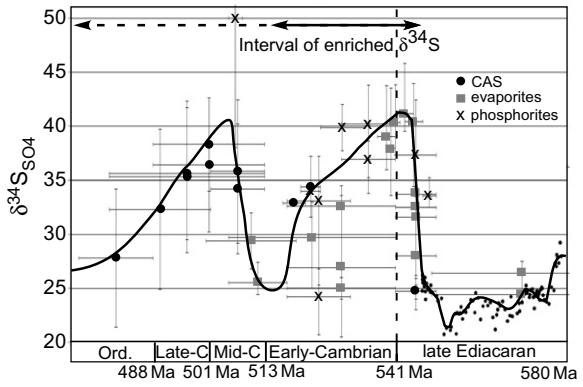

Fig. 1. Summary of enriched $\delta^{34}S_{SO_4}$ over Ediacaran–Cambrian time. $\delta^{34}S$ is plotted as the mean value reported and the vertical lines represent the total range (or standard deviation, as reported). References are as follows: CAS (Kampschulte and Strauss, 2004; Goldberg et al., 2005; Fike et al., 2006; Hurtgen, 2006); evaporites (Pisarchik and Golubchina, 1975; Claypool et al., 1980; Houghton, 1980; Strauss, 1993; Banerjee et al., 1998; Walter et al., 2000; Strauss et al., 2001; Schröder et al., 2004); phosphorites: (Shen et al., 1998; Shields et al., 1999; Shen et al., 2000; Goldberg et al., 2005; Hough et al., 2006). Age ranges have been updated to the most recent geochronological constraints where possible (Gradstein et al., 2004).

are on the order of 40‰ (Schröder et al., 2004, data presented here), whereas typical values of $\delta^{34}S_{SO_4}$ are in the range of ~15–25‰ prior to its onset (Fike et al., 2006; Kaufman et al., 2007; McFadden et al., 2008).

The Ara anomaly ushers in a period of enriched $\delta^{34}S_{SO_4}$ that lasts throughout the Cambrian (Fig. 1). Improved geochronologic constraints are needed to uniquely reconstruct seawater $\delta^{34}S_{SO_4}$ over this interval; however, it appears that there are two distinct periods of enriched $\delta^{34}S_{SO_4}$: one at E-C boundary (discussed directly in the present paper), and another during the Middle Cambrian (~510 Ma). As of this writing, it is unclear whether the mechanism(s) that caused the Ara anomaly are relevant for understanding enriched $\delta^{34}S_{SO_4}$ throughout the Early Cambrian (lasting until ca. 515 Ma) or throughout the entire early Paleozoic interval of enriched $\delta^{34}S_{SO_4}$. Even with the conservative view that the Ara anomaly terminates in the Early Cambrian, its magnitude (~20‰) and duration (⩾30 Myr) make it one of the largest known perturbations to the sulfur biogeochemical cycle in Earth history. However, an understanding of the cause of this enrichment has remained elusive. Our aim is to distinguish between possible causes (e.g., biologic vs. tectonic) for the Ara anomaly and to place the $\delta^{34}S$ record in the broader context of the evolution of Ediacaran–Cambrian biogeochemical cycling.

1.1. Geologic context

The Huqf Supergroup provides one of the best preserved, most continuous sections of Ediacaran through earliest Cambrian strata (ca. 635–540 Myr) (Amthor et al., 2003; Schröder et al., 2004). Huqf strata are preserved both in surface outcrops of the Oman Mountains and the Huqf area, and within subsurface sedimentary basins (Fig. 2). The Huqf Supergroup comprises the Abu Mahara, Nafun, and Ara groups. Stratigraphic, lithologic, and geochronologic constraints for the Huqf Supergroup are shown in Fig. 3. The Abu Mahara Group contains Marinoan-equivalent glacial deposits (Fiq Formation, ca. 635 Ma) that overlie ca. 800 Ma crystalline basement (Bowring et al., 2007). Nafun Group sediments were deposited in a regionally extensive sag basin under open, shallow marine conditions, and each formation can be traced laterally for several hundred km across Oman (Mattes and Conway-Morris, 1990; McCarron, 2000; Grotzinger et al., 2002; LeGuerroue et al., 2006). Nafun Group strata comprise two clastic-to-carbonate shallowing-upward successions (Masirah Bay Formation and Khufai Formation; Shuram Formation and Buah Formation) with an unconformity across the Khufai–Shuram boundary (McCarron, 2000) that likely includes the interval of Gaskiers glaciation at ca. 580 Ma (Bowring et al., 2007); but see LeGuerroue et al. (2006) for an alternate view. The Shuram excursion, $a > 15‰$ negative excursion in $\delta^{13}C_{carb}$, spans ~500 m of section from the basal Shuram Formation through the mid-Buah Formation (Burns and Matter, 1993; Fike et al., 2006; LeGuerroue et al., 2006). Global correlation of $\delta^{13}C_{carb}$ anomalies provides two age constraints for the Buah Formation (Fig. 3): ca. 550 Ma for the mid-Buah (correlation with Doushantuo Formation, China (Condon et al., 2005; Bowring et al., 2007)); and ca. 548 Ma for the upper Buah (correlation with Nama Group, Namibia (Grotzinger et al., 1995; Bowring et al., 2007)). These ages are consistent with those obtained directly from the overlying Ara Group.

Ara Group strata were deposited between ca. 547 and 540 Ma (Bowring et al., 2007). The Ara Group and E-C boundary strata are known definitively only from the sub-

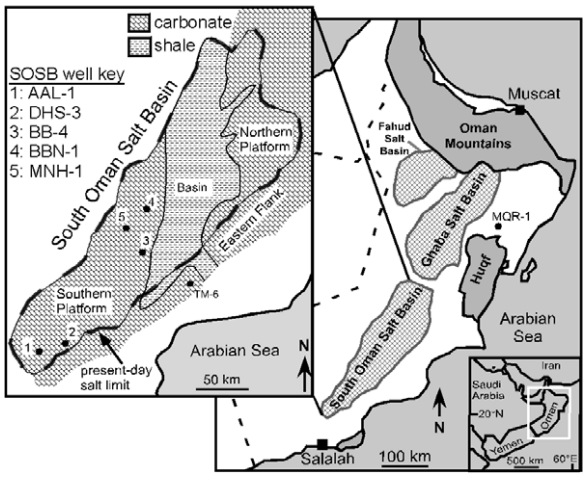

Fig. 2. Map of Oman showing locations of Neoproterozoic outcrops (dark gray). Three subsurface salt basins (Fahud, Ghaba, and South Oman Salt Basins) are indicated in the interior. The locations of the wells that provided subsurface samples are shown. Nafun Group strata were sampled from well MQR-1 located north of the Huqf region. Ara Group strata (inset) were sampled from wells that penetrate the SOSB (AAL-1, DHS-3, BB-4, BBN-1, MNH-1) or the Eastern Flank (TM-6).

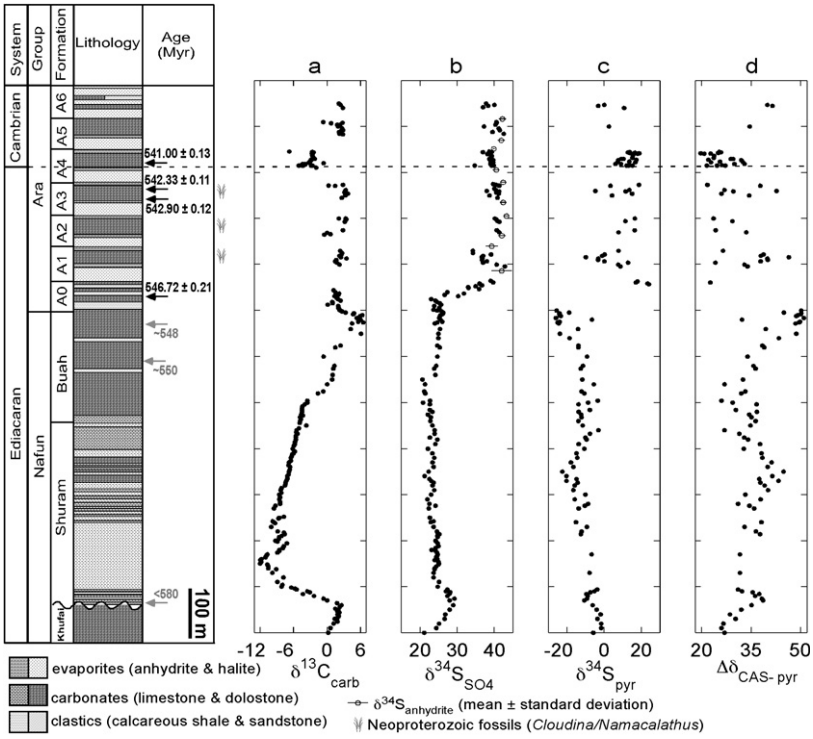

Fig. 3. Stratigraphic column for the upper Huqf Supergroup, Sultanate of Oman. The dashed line indicates the Ediacaran–Cambrian boundary. Geochronologic constraints are from single zircon U/Pb ages on ashbeds (Bowring et al., 2007). Ages in black are from Oman, those in gray are correlated to Oman based on $\delta^{13}C_{carb}$ chemostratigraphy (Fike et al., 2006). Stratigraphy consists of Nafun Group strata from MQR-1 and a compilation of all Ara SOSB data. Data from different SOSB wells are normalized to a uniform thickness for plotting purposes. (a) $\delta^{13}C_{carb}$ for reference. (b) $\delta^{34}S_{SO_4}$ from carbonate-associated sulfate (black circles). The open circles are the mean $\delta^{34}S$ for floor and roof bedded anhydrites (horizontal line through the circle is the standard deviation). (c) Pyrite $\delta^{34}S$. (d) $\Delta\delta^{34}S = \delta^{34}S_{CAS} - \delta^{34}S_{pyr}$.

surface (Mattes and Conway-Morris, 1990; Amthor et al., 2003). In strata beneath the modern day South Oman Salt Basin (SOSB), the Ara Group exists as a series of six carbonate–evaporite shallowing-upward cycles (Fig. 3), deposited in a strongly subsiding block-faulted basin (Grotzinger et al., 2002; Amthor et al., 2003; Schröder et al., 2003b). The basal Ara unit (A0) is believed to have been deposited prior to the onset of periodic basin restriction based on the absence of evaporites and/or evaporitic enrichment in e.g., $\delta^{13}C_{carb}/\delta^{18}O_{carb}$ (Amthor et al., 2003). However, it is inherently difficult to preclude the possibility of (spatially-variable) basin restriction during the Buah–Ara hiatus or contemporaneous with A0 deposition.

On the margin (termed the Eastern Flank) of the SOSB, Ara Group strata are recorded as a series of evaporite-free carbonates ~200–300 m in thickness (Fig. 4). In the absence of any preserved evaporitic strata or clear geochemical evidence (e.g., $\delta^{13}C_{carb}/\delta^{18}O_{carb}$ enrichment from basin restriction) (Amthor et al., 2003; Fike, 2007), Eastern Flank carbonate strata are interpreted to represent deposition during relative sea-level highstands (i.e., syndepositional with SOSB carbonate deposition). Evaporite deposition within the basin is then likely associated with periods of non-deposition (subaerial exposure) on the Eastern Flank. There is a robust correlation (Amthor et al., 2003) between the A4 carbonate units interbedded with evaporites on the interior of the SOSB and those deposited on the Eastern

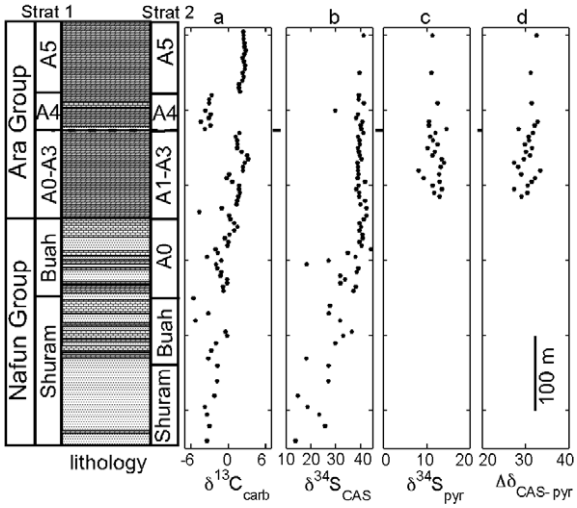

Fig. 4. Stratigraphic column for the Upper Nafun Group and the Ara Group strata of the Eastern Flank well TM-6. Existing stratigraphic assignment is indicated at left (Strat1), while a proposed revision is indicated at right (Strat2, see Fike, 2007). The dashed line indicates the Ediacaran–Cambrian boundary. The negative $\delta^{13}C_{carb}$ excursion corresponds to the A4 carbonate unit and the Ediacaran–Cambrian boundary (as in Fig. 3). Lithology follows the legend from Fig. 3. (a) $\delta^{13}C_{carb}$ for reference. (b) $\delta^{34}S_{SO_4}$ from carbonate-associated sulfate. (c) Pyrite $\delta^{34}S$. (d) $\Delta\delta^{34}S = \delta^{34}S_{CAS} - \delta^{34}S_{pyr}$.

Flank, based on the presence of an ash-bed dated to 541.0 Ma (Bowring et al., 2007), $\delta^{13}C_{carb}$ chemostratigraphy, drill core logs, and trace element geochemistry. However, the difficulty of correlating hiatal gaps in Eastern Flank strata to the periods of evaporite deposition within the SOSB hinders correlation above and below the A4 unit. Therefore, the lower Ara strata on the Eastern flank are correlated to the A0–A3 carbonate units and upper Ara strata on the Eastern flank are correlated with the A5–A6 carbonates from within the SOSB (Fig. 5). No attempt to further divide Eastern Flank strata is made. In both the SOSB and the Eastern Flank, the contact between the Buah and overlying Ara Group is marked by a disconformable, karstic surface, with Eastern Flank strata likely preserving the best record of the most basal Ara strata (Fike, 2007). The stratigraphic assignment of this portion (A0) of Eastern Flank strata (see Fig. 4) is uncertain and an alternate stratigraphic assignment is proposed (Fike, 2007).

The presence of multiple ash horizons within Ara Group strata (Fig. 3) has significantly improved our understanding of the timing and duration of Ara deposition and our ability to correlate the Oman stratigraphy with other sections globally (Grotzinger et al., 1995; Amthor et al., 2003; Bowring et al., 2007). An age of 546.72 ± 0.21 Ma from the middle of the basal Ara carbonate (A0) constrains the unconformity at the Buah–Ara contact to ~1 Myr (Bowring et al., 2007). Ash beds at the base (Amthor et al., 2003; Bowring et al., 2007) and top (Bowring et al., 2007) of the third carbonate unit (A3) yield zircon U/Pb ages of 542.90 ± 0.12 and 542.33 ± 0.11 Ma, respectively. All zircon U/Pb ages cited here are $^{206}Pb/^{238}U$ ages obtained from the same laboratory and calibrated under the same conditions, allowing for a very precise determination of the relative ages of samples (Bowring et al., 2007). These A3 ages indicate that the deposition of a typical Ara carbonate unit took ~1 Ma, consistent with the age difference between the A0 and A4 (see below) carbonates. The base of the A4 carbonate unit contains an ash that yielded a U/Pb age of 541.00 ± 0.13 Ma (Amthor et al., 2003; Bowring et al., 2007). This age, in combination with a 7‰ negative excursion in $\delta^{13}C_{carb}$ and the disappearance of Ediacaran *Namacalathus* and *Cloudina* fossil assemblages, is the basis for the identification of the E-C boundary at the base of the A4 carbonate in Oman (Amthor et al., 2003).

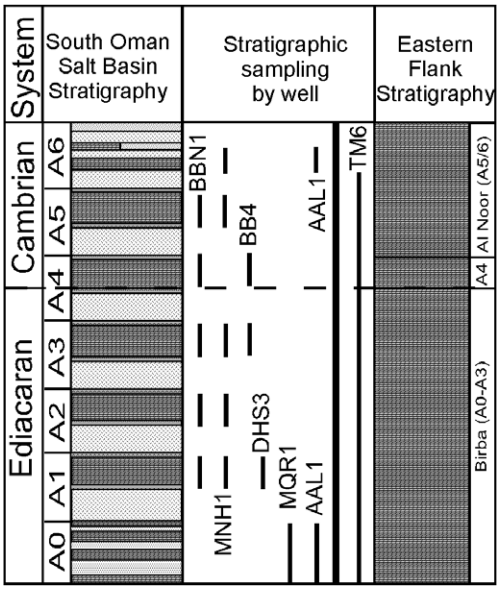

Fig. 5. Stratigraphic distribution of Ara Group samples by well from within the SOSB and the Eastern flank. The lithologic legend is the same as in Fig. 3.

2. METHODS

Samples from this study were taken as cores and cuttings from the following SOSB wells: AAL-1, BBN-1, DHS-3, BB-4, and MNH-1; as well as the Eastern Flank well TM-6 (see Electronic Annex for a complete list of samples). Cuttings are ~1–3 mm-sized fragments of rock that are collected approximately every 2 m from the borehole during drilling. As such, each sample integrates ~2 m of stratigraphy. Well locations are shown in Fig. 2 and the stratigraphic distribution of samples is shown in Fig. 5. All samples analyzed were dolomite with trace limestone in a few MNH-1 samples. Pyrite contents were typically less than 0.1 wt% sulfur and therefore unlikely to have altered the resulting CAS values significantly (Marenco et al., 2008). Results for Nafun Group strata from the well MQR-1 were reported previously (Fike et al., 2006) and are here supplemented by basal Ara strata from MQR-1 to provide context over the Nafun–Ara transition.

Samples were processed and analyzed as reported previously (Fike et al., 2006). Briefly, core samples were microdrilled to collect powder for $\delta^{13}C_{carb}/\delta^{18}O_{carb}$ analysis, while cuttings samples were crushed in a SPEX 8510 Shatterbox with an alumina ceramic container; this powder was subsampled for $\delta^{13}C_{carb}/\delta^{18}O_{carb}$ analysis. Carbonate carbon and oxygen isotopes were measured using standard methods (Ostermann and Curry, 2000). Carbon isotopes are reported as $\delta^{13}C_{carb} = (R_{standard}/R_{sample} - 1) \times 1000$, where R = the ratio of $^{13}C/^{12}C$, in units of permil (‰) relative to the V-PDB standard, while oxygen isotopes are analogously reported as $\delta^{18}O_{carb}$, relative to the V-PDB standard (see Electronic Annex). No significant isotope offset was observed between core and cuttings samples covering the same interval (see Electronic Annex).

For sulfur analysis, core samples were crushed in the SPEX 8510 shatterbox. Approximately, 10–30 g of powdered core and cuttings samples were rinsed 3× in DI to remove any water-soluble contamination. For anhydrite-bearing SOSB strata, samples were soaked repeatedly in DI to remove water-soluble sulfate minerals. The removal of water-soluble sulfates was also examined using a 10% NaCl solution (Kampschulte and Strauss, 2004), but no noticeable effect (<0.5‰ offset between treatments with and without NaCl) was observed on the resulting $\delta^{34}S_{SO_4}$ value.

Sulfate $\delta^{34}S$ was examined in the form of carbonate-associated sulfate (CAS; Burdett et al., 1989; Staudt and Schoonen, 1995; Kampschulte et al., 2001; Hurtgen et al., 2002; Kampschulte and Strauss, 2004; Gellatly and Lyons, 2005). CAS was obtained by dissolving the powdered sam-

ple in 6 N HCl for 2 h at ~60 °C under nitrogen gas or in 6 N HCl for 12–24 h at room temperature. No $\delta^{34}S$ offset was observed between these methods. Following dissolution, samples were filtered to remove insoluble residues and excess $BaCl_2$ was added to the filtrate to precipitate sulfate as $BaSO_4$. The insoluble residue was kept for pyrite analysis.

Pyrite was extracted as chromium-reducible sulfur (Canfield et al., 1986). Pyrite extraction was performed under nitrogen gas by the addition of 6 N HCl and 0.4 M reduced chromium chloride solution. The reaction was allowed to proceed for 2 h with the sulfide collected as silver sulfide after bubbling through a sodium citrate buffer (pH 4) and into a silver nitrate (0.1 M) trap. Rinsed, filtered, and dried $BaSO_4$ and Ag_2S precipitates were then combined with an excess of V_2O_5 and analyzed for S-isotope composition at Indiana University on a Finnigan MAT 252 gas source mass spectrometer fitted with a peripheral elemental analyzer (EA) for on-line sample combustion (Studley et al., 2002). Sulfur isotope compositions are expressed as $\delta^{34}S = (R_{standard}/R_{sample} - 1) \times 1000$, where R is the ratio of $^{34}S/^{32}S$, reported as permil (‰) deviations from V-CDT, with analytical error of ~0.1‰ (1σ), calculated from replicate analyses of samples and laboratory standards. Samples were calibrated using the international standards NBS-127 (20.3‰) and S3 (−31.5‰), as well as four internal standards: silver sulfide (ERE-Ag_2S: −4.3‰), chalcopyrite (EMR-CP: 0.9‰), and two barium sulfate standards (BB4-18: 39.5‰; PQB: 38.0‰).

3. RESULTS

Here we present the first high-resolution record of paired sulfate ($\delta^{34}S_{SO_4}$) and pyrite ($\delta^{34}S_{pyr}$) isotopes from Ara Group strata spanning ca. 547–540 Ma from the SOSB (Fig. 3) and Eastern Flank (Fig. 4). We place these data in the context of the Nafun Group (ca. 635–548 Ma) sulfur chemostratigraphy to discuss changes in sulfur biogeochemical cycling, and inferentially environmental change, over Ediacaran–early Cambrian time.

3.1. The ara anomaly: $^{34}S_{SO_4}$

An increase in $\delta^{34}S_{SO_4}$ in the mid-Buah Formation marks the onset of the Ara anomaly at ca. 550 Ma. Enriched $\delta^{34}S_{SO_4}$ values persist through the remainder of the Buah Formation and through the entirety of the Ara Group. This increase is observed in both the SOSB (Fig. 3b) and the Eastern Flank (Fig. 4b). The Eastern Flank strata record the full rise in $\delta^{34}S_{SO_4}$ (up to 42‰), whereas MQR-1 strata are truncated by the sub-Haima unconformity after $\delta^{34}S_{SO_4}$ has risen from 20‰ to 26‰. The sub-Haima unconformity is traceable across Oman and separates the Ara Group carbonates from the regionally extensive mid-late Cambrian Haima clastics (Millson et al., 1996). Within the SOSB, the rise in $\delta^{34}S_{SO_4}$ continues throughout the basal Ara (A0) Group, reaching values as high as 39‰ by the end of A0 deposition (ca. 546 Ma). The A0 carbonates underlie the first known evaporitic sediments and are therefore regarded as having been deposited before the basin underwent its first episode of periodic restriction (Mattes and Conway-Morris, 1990; Schröder et al., 2005; Bowring et al., 2007). $\delta^{34}S_{SO_4}$ continues to increase throughout the lower Ara units (A1–A3), reaching a maximum of 42‰ near the top of the A3 carbonate unit, just before the E-C boundary. The A4 carbonate unit (ca. 541 Ma) was deposited during the E-C boundary negative $\delta^{13}C_{carb}$ excursion, and has slightly less enriched $\delta^{34}S_{SO_4}$ (~40‰). The uppermost Ara carbonates (A5, A6) are characterized by $\delta^{34}S_{SO_4}$ averaging 41‰, indicating that elevated $\delta^{34}S$ continued into the earliest Cambrian (ca. 540 Ma). The magnitude of the Ara anomaly in $\delta^{34}S_{SO_4}$ is consistent across the SOSB itself and between the SOSB and strata of the non-evaporitic Eastern Flank, and these enriched values are consistent with reports from globally correlative sections (Fig. 1).

3.2. The ara anomaly: $\delta^{34}S_{pyr}$

Overall, there is a significant increase in $\delta^{34}S_{pyr}$, relative to typical Nafun Group values (~−15‰), associated with the enriched $\delta^{34}S_{SO_4}$ that comprises the Ara anomaly (Figs. 3c and 4c). By the basal Ara (A0), $\delta^{34}S_{pyr}$ has risen sharply to ~20‰ within strata of the SOSB. Values of $\delta^{34}S_{pyr}$ remain enriched throughout the remainder of Ara deposition (the average SOSB Ara $\delta^{34}S_{pyr}$ is 10‰). In Eastern Flank strata, pre-A4 samples from TM-6 have an average $\delta^{34}S_{pyr} = 9.3$‰; whereas $\delta^{34}S_{pyr}$ reaches 9.4‰ in A4 strata and 8.6‰ for post-A4 strata; all of which are substantially enriched relative to average $\delta^{34}S_{pyr}$ (−8‰) in TM-6 Nafun Group strata (Fike, 2007). Although not as well resolved as the $\delta^{34}S_{SO_4}$ excursion, the Ara anomaly in $\delta^{34}S_{pyr}$ is consistent across the SOSB itself and between the SOSB and the non-evaporitic Eastern Flank strata. In addition, these $\delta^{34}S_{pyr}$ values are in agreement with reports of enriched $\delta^{34}S_{pyr}$ from contemporaneous strata (Goldberg et al., 2005; Canfield et al., 2007).

The interpretation of $\delta^{34}S_{pyr}$ is complicated by its dependence on the isotopic composition of sulfate undergoing reduction and on the isotopic fractionation associated with sulfate reduction (and other microbial metabolisms) itself. It is this latter fractionation that is of interest when trying to characterize the sulfur cycle. Therefore, we focus on $\Delta\delta^{34}S = \delta^{34}S_{SO_4} - \delta^{34}S_{pyr}$ as a way to interpret variability in $\delta^{34}S_{pyr}$ decoupled from changes in $\delta^{34}S_{SO_4}$ (Figs. 3d and 4d). In the upper Nafun Group, $\Delta\delta^{34}S$ is ~32‰ in the lower Buah, and increases briefly to ~44‰ in the upper Buah coincident with the onset of enrichment in $\delta^{34}S_{SO_4}$ (Fig. 3d). These strata are interpreted to represent an interval marked by significant bacterial sulfur disproportionation (Fike et al., 2006), a microbial metabolism that can significantly increase $\Delta\delta^{34}S$ (Habicht et al., 1998). Within the SOSB (Fig. 3d), the value of $\Delta\delta^{34}S$ decreases in the basal Ara (A0), although the remainder of the Ara Group samples have an average (~27‰) that is within the range of Upper Nafun Group strata. In Eastern Flank strata, pre-A4 and A4 samples from TM-6 have an average $\Delta\delta^{34}S = 31$‰, increasing slightly to 32‰ in post-A4 strata (Fig. 4d). The greater variability in $\Delta\delta^{34}S$ in SOSB strata relative to Eastern Flank strata is attributed to the fact that

the SOSB strata are primarily samples taken from drill core (each representing ~2 cm of stratigraphy), whereas the Eastern Flank strata are exclusively samples of cuttings, which integrate ~2 m of stratigraphy. The increased stratigraphic coverage (~2 m rather than ~2 cm for core samples) for each sample of cuttings necessarily damps any high-frequency spatial variability in $\delta^{34}S_{pyr}$ and therefore $\Delta\delta^{34}S$. Despite these differences, average $\Delta\delta^{34}S$ is remarkably consistent both within the SOSB and the Eastern Flank throughout the Ara anomaly.

4. ANALYSIS AND INTERPRETATION

4.1. The ara as a record of open marine conditions

4.1.1. The $\delta^{34}S_{SO_4}$ record

Before any attempt to explain the Ara anomaly is made, we must evaluate whether these data are a record of open marine conditions (i.e., globally extensive) or the result of local basin restriction. First, we note that the onset of the Ara anomaly occurred in the open marine strata of the Nafun Group, which can be traced laterally for 100s of km (McCarron, 2000) and possess $\delta^{13}C_{carb}$ chemostratigraphy that can be correlated regionally and globally (e.g., Cozzi et al., 2004; Condon et al., 2005; Fike et al., 2006; LeGuerroue et al., 2006). The entire increase in $\delta^{34}S$ is observed in the non-evaporitic strata of the Eastern Flank (Fig. 4) and in the SOSB values as high as 39‰ are observed before the first evidence for periodic basin restriction in the Ara Group. Within the SOSB, the final ~3‰ of the Ara anomaly occurs within the A1–A3 carbonates units. These units are typically ~50–100 m in thickness and show a characteristic facies progression from outer ramp mudstones to shallow water grainstones, fossil-rich thrombolitic reefs, and peritidal carbonates. Despite being interbedded with evaporitic strata, these carbonates are believed to have been deposited under open marine conditions based on: (1) the presence of the index fossils *Cloudina* and *Namacalathus*; (2) globally correlative $\delta^{13}C_{carb}$ (Grotzinger et al., 1995; Saylor et al., 1998; Amthor et al., 2003); (3) the lack of scatter in $\delta^{13}C_{carb}$ and $\delta^{34}S_{SO_4}$ within the SOSB and between the SOSB and the Eastern Flank; (4) the facies-independence of $\delta^{34}S_{SO_4}$ (Fig. 6), which argues against local basin restriction.

Further support for open marine conditions is found in comparing the $\delta^{34}S_{SO_4}$ data from carbonate-associated sulfate in these Ara carbonate units with the stratiform anhydrite deposits that bound them (Fig. 3b, Schröder et al., 2004), which have been shown to originate from marine waters (Horita et al., 2002; Schröder et al., 2003a; Brennan et al., 2004). Despite the evaporitic conditions associated with primary evaporite deposition, stratiform anhydrite is believed to accurately record the isotopic composition of seawater sulfate because of nearly quantitative removal of seawater sulfate and the small (~1.6‰) isotopic fractionation associated with gypsum/anhydrite deposition (Raab and Spiro, 1991). It is important to note that the anhydrite layers discussed here were probably deposited as gypsum and have undergone recrystallization to anhydrite during burial. This transformation is unlikely to have altered the original $\delta^{34}S$ composition (Worden et al., 1997). A comparison of $\delta^{34}S_{SO_4}$ between carbonate-associated sulfate from the Ara carbonate units and the stratiform anhydrite deposits bounding these units (filled and open circles, respectively, in Fig. 3b) reveals that $\delta^{34}S_{anhyd}$ is enriched by ~2–4‰ with respect to the less variable $\delta^{34}S_{CAS}$. This small offset between $\delta^{34}S_{CAS}$ and $\delta^{34}S_{anhyd}$ supports an open marine interpretation for the $\delta^{34}S_{CAS}$ signal and indicates a possible minor evaporitic enrichment in $\delta^{34}S_{anhyd}$ beyond that associated with the original gypsum precipitation (Raab and Spiro, 1991). Thus, despite evidence for intermittent restriction associated with evaporite deposition, the interbedded carbonates (A1–A6) appear to have been deposited in direct connection to the global ocean.

In assessing possible restriction during deposition of the Ara Group carbonates it is most useful to compare the $\delta^{34}S_{SO_4}$ reported here with that observed in globally correlative strata. A survey of the literature finds similarly enriched sulfate ($\delta^{34}S_{SO_4} \sim 40$‰) widely distributed throughout the globe in latest Ediacaran–earliest Cambrian strata (see Fig. 1). The global pattern of enriched $\delta^{34}S$, preserved in CAS, phosphorites, and evaporites, at the time of Ara deposition strongly argues that these enriched values reflect primary seawater $\delta^{34}S_{SO_4}$, rather than being the re-

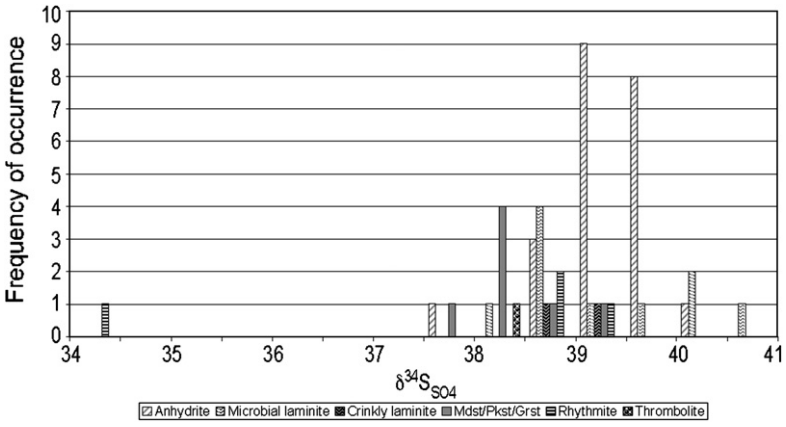

Fig. 6. Facies independence of $\delta^{34}S$ in SOSB Ara Group strata. Data are from the A3 and A4 stratigraphic units of well BB-4.

sult of multiple independently restricted basins. This provides confidence that the Ara anomaly reflects a perturbation to the global marine sulfur cycle.

4.1.2. The $\delta^{34}S_{pyr}$ record

Pyrite $\delta^{34}S$ is investigated as the geologically stable proxy for H_2S produced by bacterial sulfate reduction and/or disproportionation. $\delta^{34}S_{pyr}$ is known to depend on conditions of the local depositional environment (e.g., sedimentation rate, sulfate reduction rate, iron availability, and sulfate concentration) (Canfield, 2001). As such, in comparison to $\delta^{34}S_{SO_4}$, it is significantly more difficult to assess the likelihood that a particular range of $\delta^{34}S_{pyr}$ is representative of global marine conditions. The similarity of $\delta^{34}S_{pyr}$ between the SOSB and Eastern Flank suggest that these values (~12‰) are representative of pyrite deposition over the $\sim 10^5$ km^2 basin, despite gradients in sedimentary facies from basin margin to center. These values of $\delta^{34}S_{pyr}$ are in broad agreement with correlative sections in China (Goldberg et al., 2005) and Newfoundland (Canfield et al., 2007), spanning a range of depositional environments and lithologies from shallow to deep water, from carbonates to shales. An estimate of globally averaged $\delta^{34}S_{pyr}$ (~15‰) over this interval (compiled from the data of Canfield, 2004; Canfield et al., 2007) agrees with the average values of Ara $\delta^{34}S_{pyr}$ (~12‰) observed in this study. Therefore, following the logic outlined above for consideration of $\delta^{34}S_{SO_4}$, it is likely that the observed increase in $\delta^{34}S_{pyr}$ is representative time-equivalent strata.

4.2. Mechanisms to generate the ara anomaly

We now attempt to constrain possible causes of the Ara anomaly. In doing this, we rely on an understanding of the sulfur cycle that is based on the interpretation of high-resolution pairs of $\delta^{34}S_{SO_4}$–$\delta^{34}S_{pyr}$. For the present treatment, we restrict ourselves to a consideration of steady-state behavior (constant ocean sulfate concentration), but acknowledge that a change in sulfate concentrations can alter $\delta^{34}S_{SO_4}$ and, in particular, a decrease in sulfate levels (at constant f_{pyr}) could have contributed to the Ara anomaly by increasing $\delta^{34}S_{SO_4}$.

The steady-state equation relating the isotopic composition of sulfate in the oceans, $\delta^{34}S_{SO_4}$, and the isotopic composition of pyrite $\delta^{34}S_{pyr}$ is:

$$\delta^{34}S_{in} = (1 - f_{pyr}) * \delta^{34}S_{SO_4} + f_{pyr} * \delta^{34}S_{pyr}, \quad (1)$$

where f_{pyr} is the fraction of sulfur buried as pyrite, and $\delta^{34}S_{in}$ is the isotopic composition of sulfur entering the ocean. Analogous to similar treatments of the carbon cycle (Kump and Arthur, 1999; Rothman et al., 2003), this can be rewritten substituting $\Delta\delta^{34}S = \delta^{34}S_{SO_4} - \delta^{34}S_{pyr}$:

$$\delta^{34}S_{SO_4} = f_{pyr} * \Delta\delta^{34}S + \delta^{34}S_{in}. \quad (2)$$

It follows that the enrichment in $\delta^{34}S_{SO_4}$ observed in the Ara anomaly can be generated by varying one of these three parameters ($\Delta\delta^{34}S$, f_{pyr}, $\delta^{34}S_{in}$) (Fig. 7a,b). The first mechanism is to increase $\Delta\delta^{34}S$, the biological fractionation between coexisting sulfate and pyrite. This has the effect of enriching $\delta^{34}S_{SO_4}$ and depleting $\delta^{34}S_{pyr}$ (Fig. 7a). The second mechanism is to increase f_{pyr}, while the third mechanism is to increase $\delta^{34}S_{in}$. Both of these latter mechanisms result in a parallel enrichment of $\delta^{34}S_{SO_4}$ and $\delta^{34}S_{pyr}$ (Fig. 7b). The first two mechanisms have been commonly invoked to explain changes in $\delta^{34}S_{SO_4}$ (Claypool et al., 1980; Canfield and Teske, 1996; Halverson and Hurtgen, 2007). On the other hand, $\delta^{34}S_{in}$ is generally assumed to have been relatively invariant throughout geologic history (Garrels and Lerman, 1981; Canfield, 2001). As such, change in $\delta^{34}S_{in}$ is not typically considered as a possible

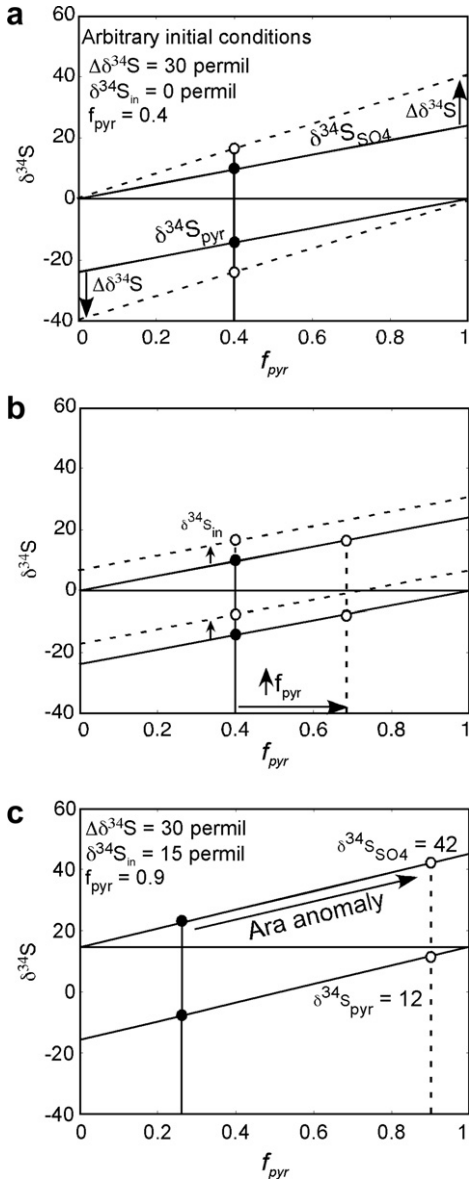

Fig. 7. (a) Increasing $\Delta\delta^{34}S$ (dashed lines, open circles) leads to increased $\delta^{34}S_{SO_4}$ and decreased $\delta^{34}S_{pyr}$ from an arbitrary initial condition. (b) Increasing f_{pyr} or $\delta^{34}S_{in}$ both lead to increased $\delta^{34}S_{SO_4}$ and increased $\delta^{34}S_{pyr}$. (c) Likely characterization of the sulfur cycle at the time of the Ara anomaly: $\delta^{34}S_{in} \sim 15$‰, and $f_{pyr} \sim 0.9$‰. An increase in $\delta^{34}S_{in}$ beyond the value shown would result in a corresponding decrease in the value of f_{pyr} needed to explain the Ara anomaly.

cause for observed $\delta^{34}S_{SO_4}/\delta^{34}S_{pyr}$ variability, although this has been proposed recently to explain unusually enriched $\delta^{34}S_{pyr}$ throughout the Neoproterozoic (Canfield, 2004). Previous attempts to identify the cause of $\delta^{34}S$ excursions in the geologic record have been hindered by the lack of coexisting $\delta^{34}S_{SO_4}$ and $\delta^{34}S_{pyr.}$ Without such data, it is not possible to rigorously identify or preclude any of these mechanisms as the cause of the observed enrichment in $\delta^{34}S_{SO_4}$ during the Ara anomaly. Using the data presented here, we now examine each of these three options in turn.

4.2.1. Increasing $\Delta\delta^{34}S$

Throughout most of the Precambrian, $\Delta\delta^{34}S$ appears to have been dominated by bacterial sulfate reduction (BSR). BSR has typical fractionations (under non-limiting sulfate conditions) of ~25‰ and an apparent maximum value of 46‰ (Canfield and Teske, 1996); but see (Brunner and Bernasconi, 2005). In the modern, and presumably throughout much of the Phanerozoic, however, there is an additional metabolism that plays a significant role in determining the overall metabolic fractionation: bacterial sulfur disproportionation (BSD). BSD is a metabolism that increases $\Delta\delta^{34}S$ through the reworking of intermediate valence (e.g., S^0, S_2O_3, SO_3^{2-}) sulfur species. As such, fractionation in the modern can reach values as high as 70‰, with average fractionations typically around 50‰ (Canfield and Teske, 1996). The apparent expression of BSD is first observed in the Mesoproterozoic (Johnston et al., 2005), although it may be far older (Philippot et al., 2007). It appears to have become more prevalent in the later Ediacaran, just after the end of the Shuram $\delta^{13}C_{carb}$ excursion (Fike et al., 2006), and is widespread throughout the Phanerozoic (Canfield and Teske, 1996). As such, based on existing data, an increase in BSD prevalence during Ara time was the most likely explanation for the increase in $\delta^{34}S_{SO_4}$ during the Ara anomaly (e.g., Canfield and Teske, 1996; Halverson and Hurtgen, 2007). Since BSD is associated with more oxidizing environments, this would be consistent with the pattern of increasing oxygenation throughout the Ediacaran (Des Marais et al., 1992; Canfield and Teske, 1996; Fike et al., 2006; Canfield et al., 2007).

However, examination of the $\delta^{34}S_{pyr}$ record (Figs. 3c and 4c) shows it tracks $\delta^{34}S_{SO_4}$, increasing to ~12‰ just before the E-C boundary. That is, with the exception of the upper Buah strata characterized by disproportionation, $\Delta\delta^{34}S$ is essentially invariant across the Ara anomaly. Nor does it seem likely, given equally enriched $\delta^{34}S_{pyr}$ in contemporaneous sections (e.g., Canfield, 2004; Goldberg et al., 2005; Canfield et al., 2007), that global $\Delta\delta^{34}S$ was significantly greater than that observed in the carbonates of the Ara Group. While we cannot rule out the existence of an unknown coeval, heavily ^{34}S-depleted pyrite sink, in the absence of any evidence for it, we find increased $\Delta\delta^{34}S$ to be an improbable explanation for the Ara anomaly. This precludes the one obviously biological explanation for the anomaly (i.e., a change in the metabolic fractionation associated with sulfur cycling). We are left to consider the remaining two hypotheses for the Ara anomaly (increased f_{pyr} and $\delta^{34}S_{in}$), both of which likely result from changes in geological and/or geochemical parameters (e.g., oceanic redox, weathering rates, riverine input) rather than direct metabolic effects.

4.2.2. Discriminating between f_{pyr} and $\delta^{34}S_{in}$

The synchronous enrichment of $\delta^{34}S_{SO_4}$ and $\delta^{34}S_{pyr}$ suggests that either f_{pyr} or $\delta^{34}S_{in}$ increased (Fig. 7b). As the Ara anomaly occurs over an interval of paleobiological significance, it is crucial to be able to distinguish between these two situations in order to correctly reconstruct the paleoenvironmental conditions during the terminal Ediacaran–earliest Cambrian.

4.3. Increased $\delta^{34}S_{in}$

4.3.1. Evidence for increased $\delta^{34}S_{in}$ during Ediacaran–Cambrian time

We argue here that, independent of any change in f_{pyr} during the Ara anomaly, $\delta^{34}S_{in}$ must have been enriched relative to modern values (~3‰) (Canfield, 2004) in latest Ediacaran–early Cambrian times, and inferentially over much of the later Proterozoic and the Paleozoic. The need for enriched $\delta^{34}S_{in}$ over the Ara anomaly is apparent on strictly mass balance considerations.

In a steady-state system, $\delta^{34}S_{in}$ must lie between average $\delta^{34}S_{SO_4}$ and average $\delta^{34}S_{pyr}$ (Fig. 7, Eq. (1)). For $\delta^{34}S_{in} = 3‰$, no value of f_{pyr} is sufficient to explain the Ara anomaly. Average values of f_{pyr} for three stratigraphic divisions with the Nafun and Ara Group are obtained by inverting Eq. (2), assuming $\delta^{34}S_{in} = 3‰$ (Canfield, 2004): Lower Nafun: 0.96; Upper Nafun: 0.56; Ara: 1.23. It is not possible for f_{pyr} to exceed unity, as that would require more than 100% of the sulfur leaving the ocean to be in the form of pyrite. Therefore, provided that Eq. (2) is a valid description of the sulfur cycle, the assumption of constant $\delta^{34}S_{in}$ (~3‰) must be wrong; in particular, $\delta^{34}S_{in} \gg 3‰$ is necessary to reconcile the data with the constraint that $f_{pyr} < 1$. Specifically, given the average values of paired $\delta^{34}S_{SO_4}$ (40‰) and $\delta^{34}S_{pyr}$ (12‰) in the Ara Group carbonates, $\delta^{34}S_{in} > 12‰$ is a necessary condition for any explanation of the Ara anomaly (Fig. 7c)—provided that the Ara $\delta^{34}S_{pyr}$ are representative of coeval pyrite isotopes. A robust estimation of $\delta^{34}S_{in}$ remains elusive at this time, but our data clearly demonstrate that the standard assumption of constant $\delta^{34}S_{in} \sim 3‰$ is not valid for the Ediacaran–Cambrian sulfur cycle.

4.3.2. Ways to generate increased $\delta^{34}S_{in}$

We now examine plausible ways to generate enriched $\delta^{34}S_{in}$ relative to bulk Earth values. Canfield (2004) proposed one such mechanism, whereby a prolonged period of ocean euxinia leads to an enrichment in average crustal $\delta^{34}S$ through the subduction of ^{34}S-depleted abyssal pyrite. Model results of prolonged pyrite subduction over the Proterozoic have yielded enrichments in $\delta^{34}S_{crust}$ up to ~70‰ prior to the oxidation of the deep ocean (Canfield, 2004). While $\delta^{34}S_{in}$ is a combination of weathering inputs (related to $\delta^{34}S_{crust}$) and mantle inputs (hydrothermal + volcanic), the weathering flux is the dominant component (Walker, 1986; Canfield, 2004). Therefore, an increase in $\delta^{34}S_{crust}$

should correspond to increased $\delta^{34}S_{in}$. This model requires widespread anoxic or euxinic conditions to increase $\delta^{34}S_{in}$, such as those thought to have been prevalent for much of the Proterozoic (Canfield, 1998; Anbar and Knoll, 2002; Poulton et al., 2004). Once the deep ocean became oxygenated, $\delta^{34}S_{in}$ would gradually return to bulk Earth values (Canfield, 2004).

We suggest an additional possible mechanism to enrich $\delta^{34}S_{in}$ by considering the preferential weathering of sulfates relative to sulfides (Berner, 2006). Sulfates weather rapidly because of their high solubility, whereas pyrites are disseminated primarily in shales and require physical weathering and erosion of the surrounding rock before they can weather under exposure to O_2 (Berner, 2006). While the weathering rate of sulfides is believed to be controlled primarily by exhumation rate, pO_2 is also thought to play a role (Jerz and Rimstidt, 2004), one that may have been more important under the low pO_2 environments of the Ediacaran (Berkner and Marshall, 1965; Canfield and Teske, 1996; Canfield et al., 2007). Indeed, recent modeling indicates that pO_2-dependent sulfide weathering is necessary to generate the $\delta^{13}C$–$\delta^{34}S$ trends observed throughout Phanerozoic strata (Bergman et al., 2004). As such, it is likely that with large isotopic offsets between sedimentarly sulfate and sulfide reservoirs, enhanced weathering of sulfates may have contributed to increased $\delta^{34}S_{in}$.

An initial enrichment of $\delta^{34}S_{in}$ through either of these pathways could be magnified by the rapid recycling of Neoproterozoic strata containing ^{34}S-enriched sulfates and pyrites. The 'rapid recycling' hypothesis (Berner, 2006) reflects the observation that young sedimentary rocks are subject to very rapid weathering relative to older strata. Estimates of weathering sources at the time of the E-C boundary suggest that both the sulfate and pyrite weathering pools are dominated by young, $\delta^{34}S$-enriched strata (Berner, 2006). In particular, the late Ediacaran was an interval of low global sea-level leading up to the Early Cambrian Sauk transgression (Matthews and Cowie, 1979). This may have further amplified any enrichment in $\delta^{34}S_{in}$ because of the preferential exposure and weathering of Ediacaran sediments known to contain both relatively ^{34}S-enriched sulfates and pyrites (Strauss, 1993; Shields et al., 1999; Canfield, 2004; Goldberg et al., 2005; Hurtgen et al., 2005; Fike et al., 2006; Hurtgen, 2006; Canfield et al., 2007).

Teasing apart these possible factors is beyond the scope of the present work, although we note that these are not mutually exclusive. Indeed it is almost certain that both pyrite subduction and preferential weathering of sulfates happened prior to the rise of atmospheric oxygen. Once these mechanisms generated an enrichment in $\delta^{34}S_{in}$ then rapid recycling of the resulting sediments could provide a positive feedback increasing $\delta^{34}S_{in}$.

4.3.3. Implications for increased $\delta^{34}S_{in}$ in older and younger strata

Variations in $\delta^{34}S_{in}$ likely operate on a time scale related to the recycling (deposition, uplift, and subsequent erosion) of marine sediments. As such, it is expected to change much slower than the residence time of sulfate in the ocean, which controls changes in $\delta^{34}S_{SO_4}$ arising from variations in both $\Delta\delta^{34}S$ and f_{pyr}. Given the slow rate of change in $\delta^{34}S_{in}$, the elevated $\delta^{34}S_{in}$ during the E-C boundary has implications for interpreting sulfur cycling both earlier in the Proterozoic and well into the Paleozoic.

The methods for enriching $\delta^{34}S_{in}$ discussed above require an isotopic offset between sulfate and sulfide sedimentary minerals (with sulfates enriched in ^{34}S relative to pyrites). As such, the efficacy of these mechanisms depends on the fractionation during sulfate reduction ($\Delta\delta^{34}S$). Thus, without an isotopic offset between sulfates and sulfides, there would be no effect on $\delta^{34}S_{in}$. Sulfate concentrations were low throughout early Earth history and therefore unlikely to generate significant $\Delta\delta^{34}S$ (Canfield, 2001; Habicht et al., 2002). It was not until the Mesoproterozoic (Shen et al., 2002; Kah et al., 2004) that sulfate concentrations rose to high enough levels ($>\sim$200 μM) to routinely generate $\Delta\delta^{34}S \gg 0$. Thus, an increase in $\delta^{34}S_{in}$ would only become possible during and after the Mesoproterozoic. Indeed, time-averaged compilations (Canfield, 2004) record a parallel rise in $\delta^{34}S_{SO_4}$ and $\delta^{34}S_{pyr}$ from approximately 1.5–0.54 Gyr. These data are consistent with increased $\delta^{34}S_{in}$ over this interval (cf. Fig. 7). Although increased pyrite burial cannot be ruled out, it seems unlikely given the general trend toward more oxidizing conditions in the Mesoproterozoic (Johnston et al., 2005).

We now consider the implications of elevated $\delta^{34}S_{in}$ for the Phanerozoic. Available data indicates that $\delta^{34}S_{SO_4}$ remains enriched throughout the Cambrian (Kampschulte and Strauss, 2004; Hough et al., 2006; Gill et al., 2007). From the Ordovician through the Permian, however, there is a nearly linear decrease in $\delta^{34}S_{SO_4}$ from $\sim$40‰ to $\sim$10‰ (Strauss, 1997; Kampschulte and Strauss, 2004). This trend dominates the Paleozoic $\delta^{34}S_{SO_4}$ curve. A parallel decrease in average $\delta^{34}S_{pyr}$ from $\sim$0‰ to $-$30‰ occurs over the same interval (Canfield, 2004). The traditional interpretation of this dramatic decline has been decreasing pyrite burial. While there is indeed evidence for a general decrease in f_{pyr} based on the decline of organic rich black shales over the Paleozoic (Berry and Wilde, 1978; Wilde, 1987; Ulmishek and Klemme, 1990; Arthur and Sageman, 1994), the magnitude of the required decrease in f_{pyr} ($\sim$80%) seems implausible and inconsistent with the rock record (Ulmishek and Klemme, 1990). Rather, we propose that the Paleozoic decrease in $\delta^{34}S_{in}$ is driven at least in part by a decrease in $\delta^{34}S_{in}$ down to near modern values ($\sim$3‰), damping the magnitude of any proposed long-term changes to f_{pyr} over the Paleozoic.

4.4. Increased f_{pyr} during the ara anomaly

Given the lack of evidence for increased $\Delta\delta^{34}S$ during this time and the relatively quick onset ($<$10 Myr) of the anomaly, which likely precludes significant change in $\delta^{34}S_{in}$, we conclude that the anomaly itself was caused primarily by an increase in f_{pyr} (Fig. 7c). For the average values of $\Delta\delta^{34}S$ ($\sim$30%) that characterize the strata prior to and during the Ara anomaly, an increase in f_{pyr} of $\sim$0.67 is necessary to enrich both $\delta^{34}S_{SO_4}$ and $\delta^{34}S_{pyr}$ by the $\sim$20‰ that characterizes the Ara anomaly (Fig. 7c). The magnitude of this change assumes that both $\delta^{34}S_{in}$ is con-

stant over this interval and that the known values of $\Delta\delta^{34}S$ reported here and in the literature are globally representative—neither of which can currently be evaluated rigorously.

This suggested increase in f_{pyr} during the latest Ediacaran follows a period that is widely regarded as representing relatively oxidizing conditions (Fike et al., 2006; Canfield et al., 2007; Kaufman et al., 2007; McFadden et al., 2008; Scott et al., in press). Given the evidence for ~580 Myr Ediacaran oxidation, how do we reconcile the apparent increase in f_{pyr} in the latest Ediacaran–earliest Cambrian? Pyrite burial is known to scale with organic carbon burial in marine systems (Morse and Berner, 1995). Burial of these reduced compounds are controlled by many factors, that group broadly into two categories, those associated with production and those associated with preservation (Berner and Raiswell, 1983; Berner, 1984; Raiswell and Berner, 1986; Arthur and Sageman, 1994).

We examine first the possibility that enhanced preservation caused the increased f_{pyr} observed in the Ara Group strata. There are two primary factors that result in enhanced preservation of pyrite: increased sedimentation rate and water-column anoxia. The control that sedimentation rate has on preservation appears to arise because increased sedimentation rate partitions sediments from the overlying pool of oxidants, minimizing remineralizaton and/or re-oxidation (Arthur and Sageman, 1994). There is evidence for increased sedimentation rates over the Ediacaran–early Paleozoic interval associated with the assembly of Gondwanaland, particularly based on the volume of quartzite sediments accumulating at this time (Squire et al., 2006). Similarly, there is a pronounced peak in $^{87}Sr/^{86}Sr$, a proxy for sedimentation rate, in the terminal Ediacaran–early Cambrian (Burns et al., 1994; Veizer et al., 1999; Halverson et al., 2007). As such, increased sedimentation rate may play a role in enhanced f_{pyr} during Ara time, but its contribution is hard to quantify in the absence of a direct measure of sedimentation rate through time.

Another factor that enhances preservation is anoxia at the site of deposition. Anoxia in the overlying waters limits the exposure of reduced materials to oxidants and, thus, increases the efficiency of organic matter and pyrite burial. The Ara Group strata contain slightly elevated TOC and pyrite relative to the upper Nafun Group (Fike, 2007), however, these signals are equivocal for resolving whether the Ara Group was affected by anoxia or increased production as both of these increase TOC and pyrite abundance (Arthur and Sageman, 1994). We turn to redox-sensitive trace element enrichments to help distinguish between these two options. Overall, Ara Group strata (with the exception of the interval spanning the E-C boundary $\delta^{13}C_{carb}$ excursion itself) show no significant enrichment in these elements (U, Re, Mo), relative to the Upper Nafun Group strata (Fike, 2007). Overall, the lack of enrichment in trace elements relative to the Upper Nafun Group suggests that redox conditions, as sampled by and recorded in Huqf strata, did not change appreciably during deposition of the Ara Group (excluding the E-C boundary itself), consistent with evidence from other terminal Ediacaran sections, where evidence for oxic conditions leading up to the E-C boundary are inferred (Kimura and Watanabe, 2001; Canfield et al., 2007; Kaufman et al., 2007; Scott et al., in press). To the degree that these local conditions can be extrapolated to a wider setting, this suggests the increase in pyrite burial is not driven by more widespread reducing conditions.

The second factor that can contribute to increased pyrite burial is an increase in primary productivity (Arthur and Sageman, 1994) or the efficiency of transporting organic carbon to the seafloor (Logan et al., 1995). Support for increased primary production at this time comes from abundant phosphorite deposits during the period of the Ara anomaly (Cook and Shergold, 1984; Brasier et al., 1997). Phosphorus is considered the limiting nutrient for productivity over geologic timescales (Tyrrell, 1999). The widespread phosphorite deposits are suggestive of enhanced biological production or organic sequestration. Elevated production is also supported by carbon isotope evidence for enhanced organic carbon burial during the latest Ediacaran–earliest Cambrian (Saylor et al., 1998). Enhanced primary production as the cause of increased pyrite burial is consistent with the continued existence of the Ediacaran fauna up until the E-C boundary. The presence of these organisms, including *Namacalathus* and *Cloudina* in the lower Ara Group carbonates and in coeval strata, has been interpreted as indicative of oxic conditions (Amthor et al., 2003). Indeed, the evolution of metazoa and the resulting increase in efficiency of organic carbon (and phosphorus) transport to the sea floor (Logan et al., 1995) may have played a key role in increasing f_{pyr} at this time. Therefore, we conclude that increased primary production and/or transport of organic carbon to the seafloor, rather than a return to more reducing conditions, was probably responsible for increased pyrite burial and thereby the onset of enriched $\delta^{34}S_{SO_4}$ during Ara deposition from ~547–540 Ma.

5. CONCLUSIONS

A unique high-resolution paired $\delta^{34}S_{SO_4}$–$\delta^{34}S_{pyr}$ dataset from the Ediacaran–early Cambrian strata of the Huqf Supergroup, Sultanate of Oman was used to constrain changes to the global sulfur cycle. A parallel enrichment of ~ 20‰ is observed in both $\delta^{34}S_{SO_4}$ and $\delta^{34}S_{pyr}$ from multiple sections between ~547 and 540 Ma. The resulting values of $\delta^{34}S_{SO_4}$ (~40‰) and $\delta^{34}S_{pyr}$ (~12‰) require that the isotopic composition of sulfur entering the ocean ($\delta^{34}S_{in}$) to be significantly enriched relative to the modern (~3‰) (Canfield, 2004). Given the near constancy of $\Delta\delta^{34}S$ over this time, the rapidity of the rise in $\delta^{34}S$ requires a significant increase (~0.67) in pyrite burial (f_{pyr}). This was likely driven by enhanced primary production in nutrient-rich waters, possibly accompanied by increased efficiency of sequestering organic carbon by biological packaging (Logan et al., 1995) and/or increased sedimentation rate (Squire et al., 2006). Future studies of paired $\delta^{34}S_{SO_4}$–$\delta^{34}S_{pyr}$ can illuminate both the temporal evolution of $\delta^{34}S_{in}$ and f_{pyr} over geologic history, as well as decipher the relationship between changes in these parameters and biological evolution.

ACKNOWLEDGMENTS

This research was supported by Petroleum Development Oman (PDO) and a grant from the Agouron Institute. D.A.F. was additionally supported by an N.S.F Graduate Research Fellowship and the MIT Global Habitability Longevity Award. We thank PDO for access to samples and logistical support, L. Pratt for use of laboratory facilities and discussions, C. Colonero, J. Fong, and S. Studley for laboratory assistance, and A. Bradley, D. Canfield, T. Dimofte, J. Eiler, D. Finkelstein, T. Lyons, A. Maloof, S. Ono, D. Rothman, R. Raiswell, J. Ries, and R. Summons for comments. Helpful reviews by M. Hurtgen, B. Gill, and an anonymous reviewer greatly improved this text.

APPENDIX A. SUPPLEMENTARY DATA

Supplementary data associated with this article can be found, in the online version, at doi:10.1016/j.gca.2008.03.021.

REFERENCES

Amthor J. E., Grotzinger J. P., Schroder S., Bowring S. A., Ramezani J., Martin M. W. and Matter A. (2003) Extinction of *Cloudina* and *Namacalathus* at the Precambrian–Cambrian boundary in Oman. *Geology* **31**, 431–434.

Anbar A. D. and Knoll A. H. (2002) Proterozoic ocean chemistry and evolution: a bioinorganic bridge? *Science* **297**, 1137–1142.

Arthur M. A. and Sageman B. B. (1994) Marine Black Shales—depositional mechanisms and environments of ancient-deposits. *Annu. Rev. Earth Planet. Sci.* **22**, 499–551.

Banerjee D. M., Strauss H., Bhattacharya S. K., Kumar V. and Mazumdar A. (1998) Isotopic composition of carbonates and sulphates, potash mineralisation and basin architecture of the Nagaur–Gangnagar evaporite basin (northwestern India) and their implications on the Neoproterozoic exogenic cycle. *Mineral. Mag.* **62A**, 106–107.

Bergman N. M., Lenton T. M. and Watson A. J. (2004) COPSE: a new model of biogeochemical cycling over Phanerozoic time. *Am. J. Sci.* **304**, 397–437.

Berkner L. V. and Marshall L. C. (1965) On the origin and rise of oxygen concentration in the Earth's atmosphere. *J. Atmos. Sci.* **22**, 225–261.

Berner R. A. (1984) Sedimentary pyrite formation: an update. *Geochim. Cosmochim. Acta* **48**, 605–615.

Berner R. A. (2006) GEOCARBSULF: a combined model for Phanerozoic atmospheric O_2 and CO_2. *Geochim. Cosmochim. Acta* **70**, 5653–5664.

Berner R. A. and Raiswell R. (1983) Burial of organic carbon and pyrite sulfur in sediments over Phanerozoic time: a new theory. *Geochim. Cosmochim. Acta* **47**, 855–862.

Berry W. B. N. and Wilde P. (1978) Progressive ventilation of the oceans—an explanation for the distribution of the lower Paleozoic black shales. *Am. J. Sci.* **278**, 257w–275w.

Bowring S. A., Grotzinger J. P., Condon D. J., Ramezani J. and Newall M. (2007) Geochronologic constraints on the chronostratigraphic framework of the Neoproterozoic Huqf Supergroup, Sultanate of Oman. *Am. J. Sci.* **307**, 1097–1145.

Brasier M., Green O. and Shields G. (1997) Ediacarian sponge spicule clusters from southwestern Mongolia and the origins of the Cambrian fauna. *Geology* **25**, 303–306.

Brennan S. T., Lowenstein T. K. and Horita J. (2004) Seawater chemistry and the advent of biocalcification. *Geology* **32**, 473–476.

Brunner B. and Bernasconi S. M. (2005) A revised isotope fractionation model for dissimilatory sulfate reduction in sulfate reducing bacteria. *Geochim. Cosmochim. Acta* **69**, 4759–4771.

Burdett J. W., Arthur M. A. and Richardson M. (1989) A Neogene seawater sulfate isotope age curve from calcareous pelagic microfossils. *Earth Planet. Sci. Lett.* **94**, 189–198.

Burns S. J., Haudenschild U. and Matter A. (1994) The strontium isotopic composition of carbonates from the late Precambrian (approximate-to-560–540 Ma) Huqf Group of Oman. *Chem. Geol.* **111**, 269–282.

Burns S. J. and Matter A. (1993) Carbon isotopic record of the latest Proterozoic from Oman. *Eclog. Geolog. Helv.* **86**, 595–607.

Canfield D. E. (1998) A new model for Proterozoic ocean chemistry. *Nature* **396**, 450–453.

Canfield D. E. (2001) Biogeochemistry of sulfur isotopes. *Rev. Mineral. Geochem.* **43**, 607–636.

Canfield D. E. (2004) The evolution of the Earth surface sulfur reservoir. *Am. J. Sci.* **304**, 839–861.

Canfield D. E., Poulton S. W. and Narbonne G. M. (2007) Late Neoproterozoic deep ocean oxygenation and the rise of animal life. *Science* **315**, 92–95.

Canfield D. E., Raiswell R., Westrich J. T., Reaves C. M. and Berner R. A. (1986) The use of chromium reduction in the analysis of reduced inorganic sulfur in sediments and shales. *Chem. Geol.* **54**, 149–155.

Canfield D. E. and Teske A. (1996) Late Proterozoic rise in atmospheric oxygen concentration inferred from phylogenetic and sulphur-isotope studies. *Nature* **382**, 127–132.

Claypool G. E., Holser W. T., Kaplan I. R., Sakai H. and Zak I. (1980) The age curves of sulfur and oxygen isotopes in marine sulfate and their mutual interpretation. *Chem. Geol.* **28**, 199–260.

Condon D., Zhu M., Bowring S., Wang W., Yang A. and Jin Y. (2005) U–Pb ages from the Neoproterozoic Doushantuo Formation, China. *Science* **308**, 95–98.

Cook P. J. and Shergold J. H. (1984) Phosphorus, phosphorites, and skeletal evolution at the Precambrian–Cambrian boundary. *Nature* **308**, 231–236.

Cozzi A., Allen P. A. and Grotzinger J. P. (2004) Understanding carbonate ramp dynamics using delta C-13 profiles: examples from the Neoproterozoic Buah Formation of Oman. *Terra Nova* **16**, 62–67.

Des Marais D. J., Strauss H., Summons R. E. and Hayes J. M. (1992) Carbon isotope evidence for the stepwise oxidation of the proterozoic environment. *Nature* **359**, 605–609.

Fike D. A. (2007) Carbon and sulfur isotopic constraints on Ediacaran biogeochemical processes, Huqf Supergroup, Sultanate of Oman. Ph.D., Massachusetts Institute of Technology.

Fike D. A., Grotzinger J. P., Pratt L. M. and Summons R. E. (2006) Oxidation of the Ediacaran Ocean. *Nature* **444**, 744–747.

Garrels R. M. and Lerman A. (1981) Phanerozoic cycles of sedimentary carbon and sulfur. *Proc. Natl. Acad. Sci. USA*, 78.

Gellatly A. M. and Lyons T. W. (2005) Trace sulfate in mid-Proterozoic carbonates and the sulfur isotope record of biospheric evolution. *Geochim. Cosmochim. Acta* **69**, 3813–3829.

Gill B. C., Lyons T. W. and Saltzman M. R. (2007) Parallel, high-resolution carbon and sulfur isotope records of the evolving Paleozoic marine sulfur reservoir. *Palaeogeogr. Palaeoclimatol. Palaeoecol.* **256**, 156–173.

Goldberg T., Poulton S. W. and Strauss H. (2005) Sulphur and oxygen isotope signatures of late Neoproterozoic to early Cambrian sulphate, Yangtze Platform, China: diagenetic constraints and seawater evolution. *Precamb. Res.* **137**, 223–241.

Gradstein F. M., Ogg J. and Smith A. (2004) *A geological time scale 2004*. Cambridge University Press, Cambridge, UK.

Grotzinger J. P., Al-Siyabi A. H., Al-Hashimi R. A. and Cozzi A. (2002) New model for tectonic evolution of Neoproterozoic–Cambrian Huqf Supergroup basins, Oman. *GeoArabia* **7**, 241.

Grotzinger J. P., Bowring S. A., Saylor B. Z. and Kaufman A. J. (1995) Biostratigraphic and geochronological constraints on early animal evolution. *Science* **270**, 598–604.

Habicht K. S., Canfield D. E. and Rethmeier J. (1998) Sulfur isotope fractionation during bacterial reduction and disproportionation of thiosulfate and sulfite. *Geochim. Cosmochim. Acta* **62**, 2585–2595.

Habicht K. S., Gade M., Thamdrup B., Berg P. and Canfield D. E. (2002) Calibration of sulfate levels in the Archean Ocean. *Science* **298**, 2372–2374.

Halverson G. P., Dudas F. O., Maloof A. C. and Bowring S. A. (2007) Evolution of the $^{87}Sr/^{86}Sr$ composition of Neoproterozoic seawater. *Palaeogeogr. Palaeoclimatol. Palaeoecol.* **256**, 103–129.

Halverson G. P. and Hurtgen M. T. (2007) Ediacaran growth of the marine sulfate reservoir. *Earth Planet. Sci. Lett.* **263**, 32–44.

Holser W. T. (1977) Catastrophic chemical events in history of ocean. *Nature* **267**, 403–408.

Horita J., Zimmermann H. and Holland H. D. (2002) Chemical evolution of seawater during the Phanerozoic: implications from the record of marine evaporites. *Geochim. Cosmochim. Acta* **66**, 3733–3756.

Hough M. L., Shields G. A., Evins L. Z., Strauss H., Henderson R. A. and Mackenzie S. (2006) A major sulphur isotope event at c. 510 Ma: a possible anoxia-extinction-volcanism connection during the Early–Middle Cambrian transition? *Terra Nova* **18**, 257–263.

Houghton M. L. (1980) Geochemistry of the Proterozoic Hormuz evaporites, Southern Iran. M.Sc. Thesis, University of Oregon.

Hurtgen M. T. (2006) Sulfur cycling in the aftermath of a Neoproterozoic (Marinoan) snowball glaciation: evidence for a syn-glacial sulfidic deep ocean. *Earth Planet. Sci. Lett.* **245**, 551–570.

Hurtgen M. T., Arthur M. A. and Halverson G. P. (2005) Neoproterozoic sulfur isotopes, the evolution of microbial sulfur species, and the burial efficiency of sulfide as sedimentary pyrite. *Geology* **33**, 41–44.

Hurtgen M. T., Arthur M. A., Suits N. S. and Kaufman A. J. (2002) The sulfur isotopic composition of Neoproterozoic seawater sulfate: implications for a snowball Earth? *Earth Planet. Sci. Lett.* **203**, 413–429.

Jerz J. K. and Rimstidt J. D. (2004) Pyrite oxidation in moist air. *Geochim. Cosmochim. Acta* **68**, 701–714.

Johnston D. T., Wing B. A., Farquhar J., Kaufman A. J., Strauss H., Lyons T. W., Kah L. C. and Canfield D. E. (2005) Active microbial sulfur disproportionation in the Mesoproterozoic. *Science* **310**, 1477–1479.

Kah L. C., Lyons T. W. and Frank T. D. (2004) Low marine sulphate and protracted oxygenation of the proterozoic biosphere. *Nature* **431**, 834–838.

Kampschulte A., Bruckschen P. and Strauss H. (2001) The sulphur isotopic composition of trace sulphates in Carboniferous brachiopods: implications for coeval seawater, correlation with other geochemical cycles and isotope stratigraphy. *Chem. Geol.* **175**, 149–173.

Kampschulte A. and Strauss H. (2004) The sulfur isotopic evolution of Phanerozoic seawater based on the analysis of structurally substituted sulfate in carbonates. *Chem. Geol.* **204**, 255–286.

Kaufman A. J., Corsetti F. A. and Varni M. A. (2007) The effect of rising atmospheric oxygen on carbon and sulfur isotope anomalies in the Neoproterozoic Johnnie Formation, Death Valley, USA. *Chem. Geol.* **237**, 47–63.

Kimura H. and Watanabe Y. (2001) Oceanic anoxia at the Precambrian–Cambrian Boundary. *Geology* **29**, 995–998.

Kump L. R. and Arthur M. A. (1999) Interpreting carbon-isotope excursions: carbonates and organic matter. *Chem. Geol.* **161**, 181–198.

Le Guerroue E., Allen P. A. and Cozzi A. (2006) Chemostratigraphic and sedimentological framework of the largest negative carbon isotopic excursion in Earth history: the Neoproterozoic Shuram Formation (Nafun Group, Oman). *Precamb. Res.* **146**, 68–92.

Logan G. A., Hayes J. M., Hieshima G. B. and Summons R. E. (1995) Terminal proterozoic reorganization of biogeochemical cycles. *Nature* **376**, 53–56.

Marenco P. J., Corsetti F. A., Hammond D. E., Kaufman A. J. and Bottjer D. J. (2008) Oxidation of pyrite during extraction of carbonate associated sulfate. *Chem. Geol.* **247**, 124–132.

Mattes B. W. and Conway-Morris S. (1990) Carbonate/evaporite deposition in the Late Precambrian–Early Cambrian Ara Formation of southern Oman. In *The Geology and Tectonics of the Oman Region* (eds. A. H. F. Robertson, M. P. Searle and A. C. Ries). Geological Society, London.

Matthews S. C. and Cowie J. W. (1979) Early Cambrian transgression. *J. Geol. Soc.* **136**, 133–135.

McCarron G. (2000) The sedimentology and chemostratigraphy of the Nafun Group, Huqf Supergroup, Oman. Ph.D. Thesis, Oxford University, p. 175.

McFadden K. A., Huang J., Chu X., Jiang G., Kaufman A. J., Zhou C., Yuan X. and Xiao S. (2008) Pulsed oxidation and biological evolution in the Ediacaran Doushantuo Formation. *Proc. Natl. Acad. Sci. USA* **105**, 3197–3202.

Millson J. A., Mercadier C. G. L., Livera S. E. and Peters J. M. (1996) The Lower Palaeozoic of Oman and its context in the evolution of a Gondwanan continental margin. *J. Geol. Soc.* **153**, 213–230.

Morse J. W. and Berner R. A. (1995) What determines sedimentary C/S ratios? *Geochim. Cosmochim. Acta* **59**, 1073–1077.

Ostermann D. R. and Curry W. B. (2000) Calibration of stable isotopic data: an enriched $\delta^{18}O$ standard used for source gas mixing detection and correction. *Paleoceanography* **15**, 353–360.

Philippot P., Van Zuilen M., Lepot K., Thomazo C., Farquhar J. and Van Kranendonk M. J. (2007) Early Archaean microorganisms preferred elemental sulfur, not sulfate. *Science* **317**, 1534–1537.

Pisarchik Y. K. and Golubchina M. N. (1975) Sulfur isotope composition for Cambrian calcium sulfates from the Siberian platform. *Geochem. Int.* **8**, 227–230.

Poulton S. W., Fralick P. W. and Canfield D. E. (2004) The transition to a sulphidic ocean ~1.84 billion years ago. *Nature* **431**, 173–177.

Raab M. and Spiro B. (1991) Sulfur isotopic variations during seawater evaporation with fractional crystallization. *Chem. Geol.* **86**, 323–333.

Raiswell R. and Berner R. A. (1986) Pyrite and organic matter in Phanerozoic normal marine shales. *Geochim. Cosmochim. Acta* **50**, 1967–1976.

Rothman D. H., Hayes J. M. and Summons R. E. (2003) Dynamics of the Neoproterozoic carbon cycle. *Proc. Natl. Acad Sci. USA* **100**, 8124–8129.

Saylor B. Z., Kaufman A. J., Grotzinger J. P. and Urban F. (1998) A composite reference section for terminal Proterozoic strata of southern Namibia. *J. Sedim. Res.* **68**, 1223–1235.

Schröder S. and Grotzinger J. P. (2007) Evidence for anoxia at the Ediacaran–Cambrian boundary: the record of redox-sensitive

trace elements and rare earth elements in Oman. *J. Geol. Soc.* **164**, 175–187.

Schröder S., Grotzinger J. P., Amthor J. E. and Matter A. (2005) Carbonate deposition and hydrocarbon reservoir development at the Precambrian–Cambrian boundary: the Ara Group in South Oman. *Sedim. Geol.* **180**, 1–28.

Schröder S., Schreiber B. C., Amthor J. E. and Matter A. (2003a) A depositional model for the terminal Neoproterozoic–Early Cambrian Ara Group evaporites in south Oman. *Sedimentology* **50**, 879–898.

Schröder S., Schreiber B. C., Amthor J. E. and Matter A. (2003b) A depositional model for the terminal Neoproterozoic–Early Cambrian Ara Group evaporites in south Oman. *Sedimentology* **50**, 879–898.

Schröder S., Schreiber B. C., Amthor J. E. and Matter A. (2004) Stratigraphy and environmental conditions of the terminal Neoproterozoic–Cambrian period in Oman: evidence from sulphur isotopes. *J. Geol. Soc.* **161**, 489–499.

Scott C., Lyons T. W., Bekker A., Shen Y., Poulton S. W., Chu X. and Anbar A. D. (in press) Tracing stepwise oxygenation of the Proterozoic biosphere. *Nature*.

Shen Y., Canfield D. E. and Knoll A. H. (2002) Middle Proterozoic ocean chemistry: evidence from the McArthur Basin, Northern Australia. *Am. J. Sci.* **302**, 81–109.

Shen Y., Schidlowski M. and Chu X. (2000) Biogeochemical approach to understanding phosphogenic events of the terminal Proterozoic to Cambrian. *Palaeogeogr. Palaeoclimatol. Palaeoecol.* **158**, 99–108.

Shen Y. N., Zhao R., Chu X. L. and Lei J. J. (1998) The carbon and sulfur isotope signatures in the Precambrian–Cambrian transition series of the Yangtze Platform. *Precamb. Res.* **89**, 77–86.

Shields G. A., Strauss H., Howe S. S. and Siegmund H. (1999) Sulphur isotope compositions of sedimentary phosphorites from the basal Cambrian of China: implications for Neoproterozoic–Cambrian biogeochemical cycling. *J. Geol. Soc.* **156**, 943–955.

Squire R. J., Campbell I. H., Allen C. M. and Wilson C. J. L. (2006) Did the Transgondwanan Supermountain trigger the explosive radiation of animals on Earth? *Earth Planet. Sci. Lett.* **250**, 116–133.

Staudt W. J. and Schoonen M. A. A. (1995) Sulfate incorporation into sedimentary carbonates. In *Geochemical Transformations of Sedimentary Sulfur* (eds. M. A. Vairavamurthy, M. A. A. Schoonen, T. I. Eglinton, G. W. Luther III, B. Manowitz). *ACS Symposium Series*, Washington, DC, United States.

Strauss H. (1993) The sulfur isotopic record of Precambrian sulfates—new data and a critical-evaluation of the existing record. *Precamb. Res.* **63**, 225–246.

Strauss H. (1997) The isotopic composition of sedimentary sulfur through time. *Palaeogeogr. Palaeoclimatol. Palaeoecol.* **132**, 97–118.

Strauss H., Banerjee D. M. and Kumar V. (2001) The sulfur isotopic composition of Neoproterozoic to early Cambrian seawater—evidence from the cyclic Hanseran evaporites, NW India. *Chem. Geol.* **175**, 17–28.

Studley S. A., Ripley E. M., Elswick E. R., Dorais M. J., Fong J., Finkelstein D. and Pratt L. M. (2002) Analysis of sulfides in whole rock matrices by elemental analyzer-continuous flow isotope ratio mass spectrometry. *Chem. Geol.* **192**, 141–148.

Thode H. G. and Monster J. (1965) Sulfur-isotope geochemistry of petroleum, evaporites, and ancient seas. In *Fluids in Subsurface Environments* (eds. A. Young, J. E. Galley). AAPG, Tulsa.

Tyrrell T. (1999) The relative influences of nitrogen and phosphorus on oceanic primary production. *Nature* **400**, 525–531.

Ulmishek G. F. and Klemme H. D. (1990) *Depositional Controls, Distribution, and Effectiveness of World's Petroleum Source Rocks*. US Geological Survey, Washington, DC.

Veizer J., Ala D., Azmy K., Bruckschen P., Buhl D., Bruhn F., Carden G. A. F., Diener A., Ebneth S., Godderis Y., Jasper T., Korte G., Pawellek F., Podlaha O. G. and Strauss H. (1999) $^{87}Sr/^{86}Sr$, $\delta^{13}C$, and $\delta\ ^{18}O$ evolution of Phanerozoic seawater. *Chem. Geol.* **161**, 59–88.

Walker J. C. G. (1986) Global geochemical cycles of carbon, sulfur and oxygen. *Mar. Geol.* **70**, 159–174.

Walter M. R., Veevers J. J., Calver C. R., Gorjan P. and Hill A. C. (2000) Dating the 840–544 Ma Neoproterozoic interval by isotopes of strontium, carbon, and sulfur in seawater, and some interpretative models. *Precamb. Res.* **100**, 371–433.

Wilde P. (1987) Model of progressive ventilation of the late Precambrian–early Paleozoic ocean. *Am. J. Sci.* **287**, 442–459.

Worden R. H., Smalley P. C. and Fallick A. E. (1997) Sulfur cycle in buried evaporites. *Geology* **25**, 643–646.

Associate editor: Timothy W. Lyons